PAPER Special Issue on Radar Technology

# High-Resolution Radar Image Reconstruction Using an Arbitrary Array

Toshio WAKAYAMA†, Toru SATO† *and* Iwane KIMURA†, *Members*

**SUMMARY** Radar imaging technique is one of the most powerful tool for underground detection. However, performance of conventional methods is not sufficiently high when the observational direction or the aperture size is restricted. In the present paper, an image reconstruction method based on a model fitting with nonlinear least-squares has been developed, which is applicable to arbitrarily arranged arrays. Reconstruction is executed on the assumption that targets consist of discrete point scatterers embedded in a homogeneous medium. Model fitting is iterated as the number of point target in the assumed model is increased, until the residual in fitting becomes unchanged or small enough. A penalty function is used in nonlinear least-squares to make the algorithm stable. Fundamental characteristics of the method revealed with computer simulation are described. This method focuses a much sharper image than that obtained by the conventional aperture synthesis technique.

***key words:*** *radar, image reconstruction, model fitting, nonlinear least-squares, underground detection*

## 1. Introduction

Radar image reconstruction technique has been applied to various fields including the underground detection. Diffraction tomography is one of the methods, which reconstructs an image in the real space by Fourier transforming data obtained in the wavenumber space. When targets are observed from all directions, diffraction tomography reconstructs a fine image. However, if the observational direction is restricted, the reconstructed image deteriorates seriously because of the deficit occurred in the wavenumber region. Therefore an appropriate interpolation must be executed before the image reconstruction with diffraction tomography. Although various interpolation methods have been developed for diffraction tomography [1], [2], these do not work well when the deficit region is too large.

In order to directly avoid the problem of deficit, we have developed a reconstruction algorithm without using Fourier transform, which can be applied to an arbitrarily arranged array. This algorithm is based on a model fitting with nonlinear least-squares on the assumption that targets consist of point scatterers embedded in a homogeneous medium. Similar optimization techniques are also used to solve inverse problems for such as seismic modeling [3] and reconstruction of a profile of layered media [4]-[6]. In the present paper, we show the principle of the algorithm and the fundamental characteristics revealed by a series of computer simulation. We also quantitatively compare our algorithm with the conventional aperture synthesis method and show the advantage of the proposed method.

Manuscript received April 30, 1993.
Manuscript revised June 10, 1993.

† The authors are with the Faculty of Engineering, Kyoto University, Kyoto-shi, 606-01 Japan.

## 2. Simulation Model

Figure 1 illustrates the simulation model used in this study. A simple two-dimensional model is adopted in order to examine the fundamental characteristics of the inverse scattering problem treated in the image reconstruction. Five omni-directional antennas which are used both for transmission and reception are located at a fixed interval, and 25 time series data can be obtained with all combinations of these transmitters and receivers. Targets are assumed to consist of point scatterers with isotropic scattering characteristics. These targets are embedded in a homogeneous medium which has low-pass frequency characteristics. A monocycle pulse is transmitted, scattered by targets, and received by receivers. The received waveform is determined by the frequency characteristics of the transmitter, the receiver, the scatterer and the medium. Our algorithm reconstructs an image on the assumption that the overall frequency characteristics are known. In this paper, the received waveform is determined in the following way. According to the basic equation of diffraction tomography [7], the electric field of the scattered wave at wavenumber $k$ is

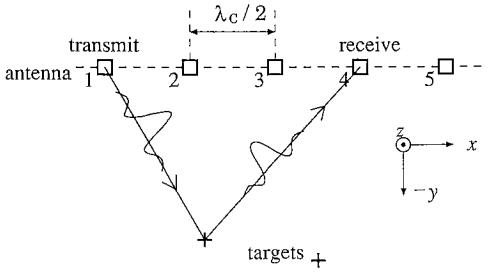


**Fig. 1** Simulation model.

$$e^s_{tr}(k) = -\frac{k^2}{16}\iint \gamma(x, y)\, H_0^{(1)}(k|\boldsymbol{r}_t - \boldsymbol{r}|) \cdot H_0^{(1)}(k|\boldsymbol{r}_r - \boldsymbol{r}|)\, dxdy \quad (1)$$

where $\boldsymbol{r}_t$ and $\boldsymbol{r}_r$ are positions of transmitters and receivers, respectively, and $\gamma$ is the reflection coefficient. $H_0^{(1)}$ is Hankel function which is the two dimensional Green's function in free space. When targets consist of $N$ point scatterers, integral of Eq. (1) can be replaced by a summation as

$$e^s_{tr}(k) = -\frac{k^2}{16}\sum_{i=1}^{N} \gamma_i H_0^{(1)}(k|\boldsymbol{r}_t - \boldsymbol{r}_i|)\, H_0^{(1)}(k|\boldsymbol{r}_r - \boldsymbol{r}_i|). \quad (2)$$

where $\gamma_i$ is the reflection coefficient of the $i$-th target. $\gamma_i$ is assumed to be independent of frequency. We assume that the frequency characteristic at low frequency is represented by Eq. (2). Since the received wave also has a high frequency characteristics, a smoothly decaying characteristic is set above a fixed high-cutoff frequency whose wavelength is $\lambda_c$. The interval between antennas is chosen as $\lambda_c/2$ in the following computation.

## 3. Initial Value Determination

Since nonlinear least-squares is an iterative method, appropriate initial values for target parameters to be estimated must be provided in order to assure that the parameters converge to correct values. In this study, initial values are determined with delay times and phases of pulses in the received time series data obtained with each combination of a transmitter and a receiver.

In the first step, information on parameters of targets are extracted from each of these received time series data. An instantaneous envelope [8] of the received raw time series data is computed in order to determine the delay and the phase of each pulse. Figure 2 is an example of the simulated received time series data. The thin line is the raw data, and the thick line shows the instantaneous envelope. This envelope has two prominent peaks, which indicates that the received wave contains scattered waves from two point targets. The position of each peak of the envelope, i.e. the delay time of each pulse determines the one-dimensional position of the corresponding target.

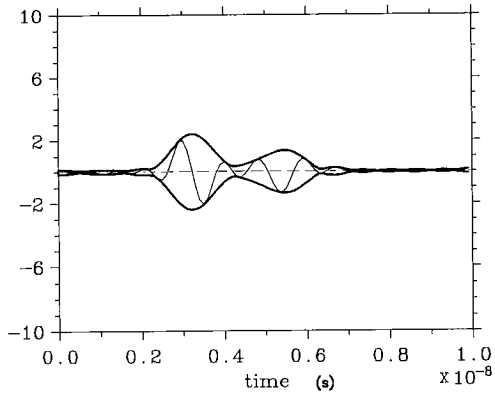


**Fig. 2** Simulated received time series data. The thin line is the raw data and the thick line is the instantaneous envelope.

A pulse scattered by a point target has a differential waveform of the transmitted pulse [9]. In the simulation, a wave scattered by a target with reflection coefficient of a real number has an odd functional waveform, whereas a wave scattered by a target with reflection coefficient of a purely imaginary number has an even functional wave form. Therefore these waveforms are orthogonal with each other. In general a reflection coefficient has both real and imaginary components, and thus these components of the reflection coefficient must be separately determined. If the waveform of the received pulse is $f(t)$, the reflection coefficient $\gamma = \gamma^{(r)} + j\gamma^{(i)}$ is calculated from the following equation:

$$\gamma^{(r)} = \frac{\int f(t)\, s^{(r)}(t)\, dt}{\int \{s^{(r)}(t)\}^2 dt} \quad (3)$$

$$\gamma^{(i)} = \frac{\int f(t)\, s^{(i)}(t)\, dt}{\int \{s^{(i)}(t)\}^2 dt} \quad (4)$$

where $s^{(r)}$ is a wave scattered by a target with a real reflection coefficient and with the same delay time as $f(t)$, and $s^{(i)}$ is a wave scattered by a target with a purely imaginary reflection coefficient. In Fig. 2, the pulse with the delay time of 32 ns has an odd functional waveform. Thus we can estimate that the reflection coefficient of the corresponding target is real. On the other hand, the pulse with 55 ns delay has an even functional waveform and therefore the corresponding target is estimated to have a reflection coefficient of purely imaginary. If two pulses are observed at close points on the time axis, interference between the two pulses may cause an error of phase estimate. Such error is recovered by the nonlinear least-squares described in the next section.

In the next step, the two-dimensional position of targets are determined by combination of the one-dimensional positions obtained from all time series data. Let a delay time of a pulse be $t_d$. The target corresponding to the delay $t_d$ is located on the ellipse of semi-major axis $ct_d/2$ ($c$ is the speed of light in the medium) with two focuses at the positions of the transmitter and the receiver. Two different ellipses can be drawn from a different set of two time series data, and we can determine the location of the intersection of these two ellipses. Symbols ○ in Fig. 3 indicate the positions of such intersections calculated from all

combinations of received time series data. The intersections prominently concentrate at two points, so that we can easily judge that two targets exist in the observational region. Some intersections are located at wrong positions. These errors are due to combinations of delay values of pulses scattered by different targets.

In order to select correct positions of targets, we define the degree of concentration of estimated points. The degree of concentration is calculated by counting the neighboring intersections with Gaussian weight at grid points set in the whole observational region, and is given by

$$C_j=\sum_{i=1}^{N}\exp\left\{-\frac{(x_i-x_j)^2+(y_i-y_j)^2}{r_0^2}\right\} \tag{5}$$

where $(x_i, y_i)$ is the position of an intersection of two ellipses, $N$ is the number of intersections, $(x_j, y_j)$ is the position of the grid point, and $r_0$ determines the width of the Gaussian weighting function. We empirically set $r_0=\lambda_c/4$ so that it does not reduce the resolution. The contour of Fig. 4 illustrates the degree of concentration computed from Fig. 3. We can clearly identify two targets and roughly estimate their positions.

The result of the process described in this section is used as an initial guess for the nonlinear least-squares fitting.

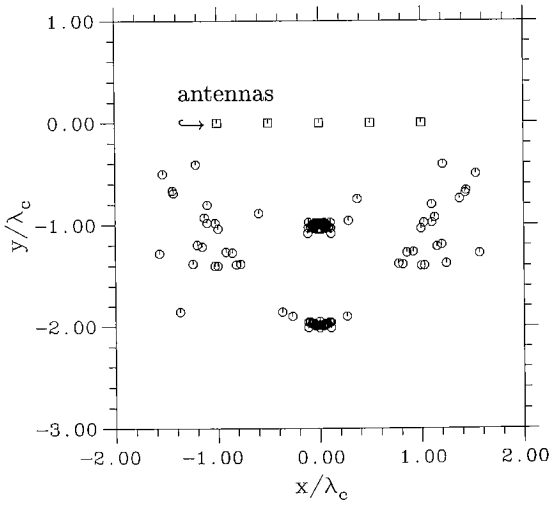


**Fig. 3** Determination of initial values of parameters to be estimated. Symbols □ and ○ indicate the location of antennas and intersections, respectively.

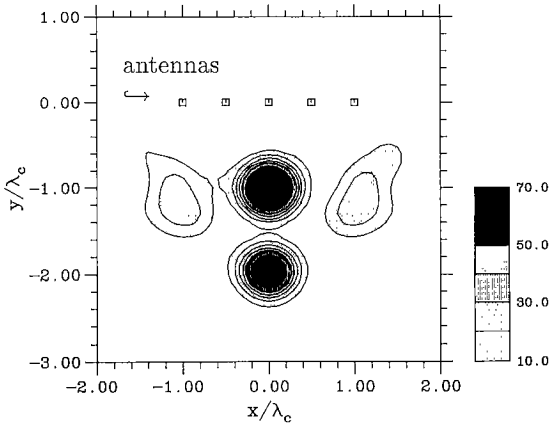


**Fig. 4** Distribution of the degree of concentration.

## 4. Nonlinear Least-Squares Fitting

The estimated electric field of a scattered wave is expressed as

$$e_{tr}^{e}(k)=-\frac{k^2}{16}\sum_{i=1}^{N^e}\gamma_i^e H_0^{(1)}(k|\boldsymbol{r}_t-\boldsymbol{r}_i^e|)\cdot H_0^{(1)}(k|\boldsymbol{r}_r-\boldsymbol{r}_i^e|) \tag{6}$$

where superscript $e$ denotes the estimated parameters. The error of the estimation is expressed as

$$F=\sum_{t,r,j}(|e_{tr}(k_j)-e_{tr}^{e}(k_j)|^2). \tag{7}$$

Nonlinear least-squares algorithm estimates the parameters of the targets by minimizing the error $F$. Among several kinds of nonlinear least-squares method, the modified Marquardt method [10] is adopted here.

The ability of separating two point targets is determined by the bandwidth of the received pulse, or the pulse width. If two peaks corresponding to two targets overlap each other in the received time series data, and therefore cannot be separated even with any combination of a transmitter and a receiver, the algorithm cannot separate two targets.

The ability of separation is evaluated in Fig. 5 from this point of view. In this figure, each boundary of the region enclosed by the solid line is made of some arcs. Each of these arcs is a part of a circle with a center of each position of the antenna and with radius of $l+\lambda_c/4$ or $l-\lambda_c/4$ where $l$ is the distance between

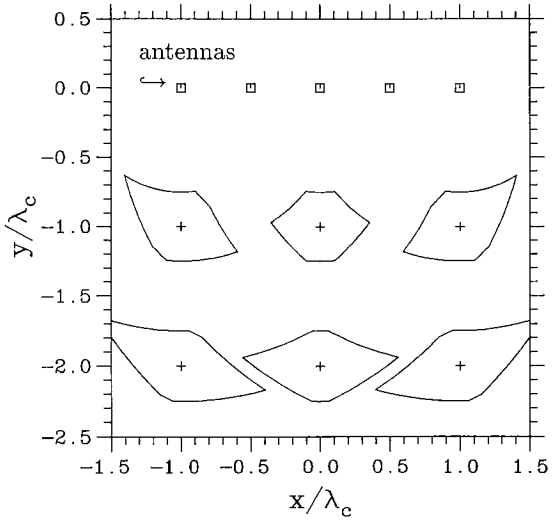


**Fig. 5** Ability to separate two point targets.

the antenna and the target. To make the problem simple, the form of the region is calculated from only mono-static observations with the antennas 1, 3, and 5, which are sufficient to represent the approximate form. If a target exists at a position indicated by + in the figure, the algorithm cannot separate this target from another target within the region.

## 5. Iteration Algorithm

The model fitting with nonlinear least-squares can reconstruct an accurate image if distance between targets is large enough. If not, some targets may not be detected in determining initial values. This problem is partly solved by iterating the combination of initial-value determination and nonlinear least-squares. Figure 6 illustrates the algorithm of the iteration method. In this section, the algorithm of the iteration method is described with an example shown in Fig. 7. Figure 7 (a) is the true image of 4 point targets. $x$ and $y$ axes represent the location of targets and antennas, and $z$ axis represents the magnitude of targets. Figure 7 (b) is the result of executing a single sequence of initial value determination and nonlinear least-squares. Only one target near the antenna array is detected. This is because scattered wave from other 3 targets are buried in the wave of the detected target, and thus the algorithm of initial value determination cannot detect all targets. Concerning the detected target, however, accurate estimation is made on its location and magnitude. It is thus possible to obtain echoes from weaker targets by subtracting the estimated time series data from the original time series data. This process yields the residual time series data, where the pulses of undetected targets come out. Then the same algorithm for the determination of initial values as described before is applied to this residual data. Since the most of the effect of the largest target is removed from the residual time series, a target with a smaller contribution can be detected. Then by using the parameters of all the detected targets, including these for previously detected targets, the nonlinear least-squares fitting revises the target image. This iteration is repeated until the residual becomes small enough or unchanged. Figures 7 (c), (d) are the result of iteration. The number of detected target increases with increasing iteration, and all targets can be detected and precisely estimated by the third iteration. The result also shows that the excessive iteration do not change the reconstructed image.

Although the antennas are linearly located in the simulation previously described, the fitting algorithm can be applied to an arbitrarily arranged array since the algorithm has no restriction on the array configuration. For example, when the antenna array

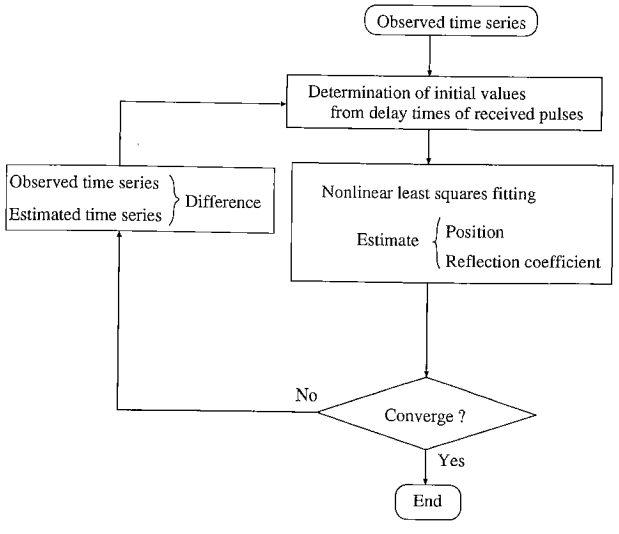


**Fig. 6** Block diagram of the iteration algorithm.

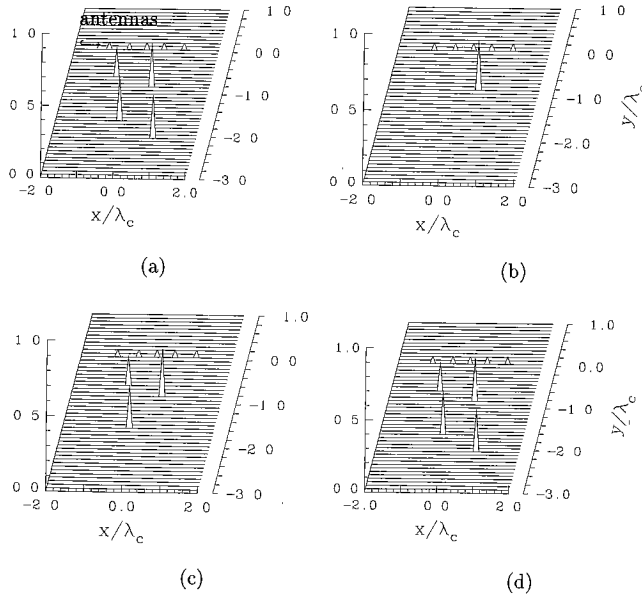


**Fig. 7** Image reconstruction by the iteration algorithm.
(a) the true image of the targets, (b), (c), (d) the reconstructed image at loop 1, 2, 3, respectively.

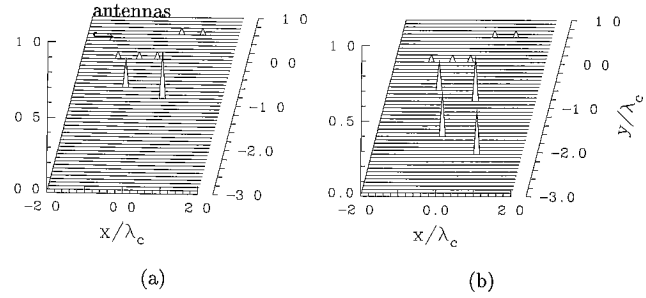


**Fig. 8** An example of a reconstruction by a nonlinear array. The antenna array has a step shape.
(a) loop=1, (b) loop=2.

has a step shape as shown in Fig. 8, the fitting algorithm can reconstruct the image without any problem. On the other hand, the diffraction tomography by cylindrical wave can be applied only when the shape of the antenna array is linear. In the actual observation, there are many cases where the locations of the antennas are restricted. However, the proposed algorithm needs some conditions on antenna location to keep the performance. In order not to produce grating false image, the interval of antennas should be less than $\lambda_c/2$. Moreover, the aperture size of the array should be larger than the wavelength. If these conditions are satisfied, the proposed algorithm is applicable to arbitrarily arranged array, and thus this algorithm is more flexible than the diffraction tomography from this point of view.

## 6. Stable Reconstruction with Penalty Function

The simulation model described in the previous section included no clutter echoes. If the clutter level is high, residual does not become small enough and the iteration algorithm may become unstable. In such a case, many spurious images appear as the iteration goes on.

A typical spurious image appears in the form of a pair of two targets with almost identical magnitude and with opposite phase with each other. Because the scattered waves from these two targets cancels each other, the pair of the targets has no contribution to the received time series data.

Considering this nature of the spurious images, we can avoid the instability by making an assumption that such a pair of anti-phase targets does not exist in the real data. It is realized by adding a penalty function $P(\boldsymbol{r}_1^e, \cdots, \boldsymbol{r}_{Ne}^e)$ to the residual:

$$F=\sum_{t,r,j}(|e_{tr}(k_j)-e_{tr}^e(k_j)|^2)+\{w_pP(\boldsymbol{r}_1^e, \cdots, \boldsymbol{r}_{Ne}^e)\}^2 \tag{8}$$

where $w_p$ is the weight. This function is chosen to become large when the distance of any two targets become short, so that the nonlinear least-squares algorithm keeps a certain distance between arbitrary two targets, preventing the algorithm from converging to a spurious solution. In this study, the penalty function is defined as follows:

$$P(\boldsymbol{r}_1^e, \cdots, \boldsymbol{r}_{Ne}^e)=\sum_{i\neq j}\frac{\exp(-0.5(r_{ij}/r_0)^2)}{(r_{ij}/r_0)} \tag{9}$$

where $r_{ij}$ is the distance between $i$-th and $j$-th targets. Here we set $r_0$ to $0.2\lambda_c$ and the weight $w_p$ is adjusted to a value which makes the terms of residual and penalty function have comparable magnitudes.

Figure 9 illustrates the effect of the penalty function. In this simulation, small scatterers of clutter sources are distributed around one target as shown in Fig. 9 (a). They are distributed at the rate of one scatterer per a $(\lambda_c/2)\times(\lambda_c/2)$ square, that is, the rate of about one scatterer per one resolution cell. We define Signal to Interference Ratio (SIR) as the ratio of the magnitude of the minimum target to the standard deviation of clutters. The SIR in the example of Fig. 9 is 20 dB. Although spurious responses emerge in the image without the penalty function, as shown in Fig. 9 (b), they disappear after the addition of the penalty function, and stable reconstruction is made as shown in Fig. 9 (c).

Figure 10 shows the transition of residuals in the case of various interference levels. The target model is the same as shown in Fig. 7 (a), which includes 4 point targets. When the clutter does not exist, the algorithm detects all 4 targets at the third iteration where the residual suddenly decreases. The excessive iteration does not change the residual and the reconstructed image. The final level of residual increases as SIR decreases, or the clutter level increases, and consequently the minimum level of the detectable magnitude of a target becomes larger. When the SIR is 20 dB, the

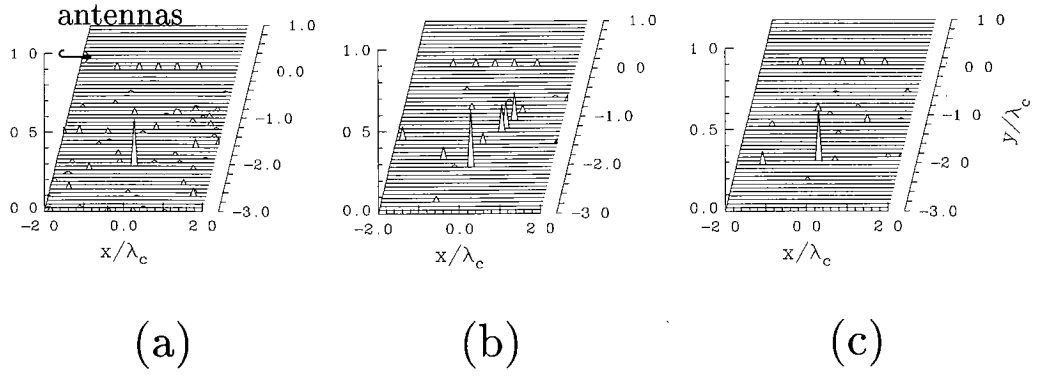


**Fig. 9** Stabilization with penalty function.
(a) the true image of the targets.
(b) the reconstruction image without using the penalty function.
(c) the reconstruction image with the penalty function.

residual increases at 5th iteration. This is because the weight of penalty function is a little larger than the optimum value. Even in this case, the algorithm also detects all 4 targets at the second iteration and excessive iteration hardly changes the reconstructed image.

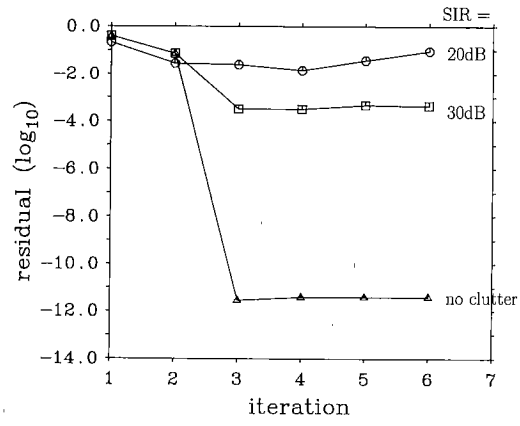


**Fig. 10** Transition of the residual in the case of various interference levels.

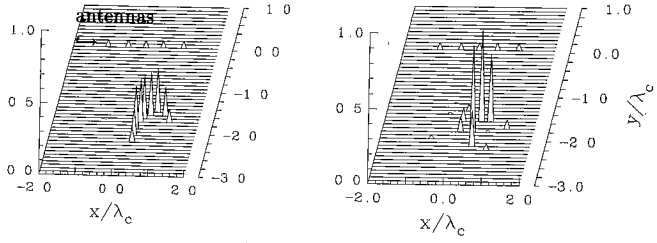


(a) (b)

**Fig. 11** Reconstruction of the image of the target with a finite size.
(a) the true image represented by 9 point targets.
(b) the reconstructed image at loop=5.

Penalty function is also effective when the observed target has a finite size. Figure 11 shows a result of applying the same fitting algorithm to a target with a finite size, where the simulated data is calculated from the model shown by Fig. 11(a). On the basis of the equivalent source method [11], this model consists of 9 point targets which approximately represents the cylindrical target whose upper side is illuminated by the transmitter.

As the iteration of the fitting algorithm goes on, the number of point targets increases, and by the 5th iteration the target image is reconstructed as shown in Fig. 11(b). In this reconstruction, the penalty function, whose width $r_0$ is set to $0.1\lambda_c$, keeps the proper distances between the assumed point targets and help them to represent the approximate shape of the real target. Although the performance of this reconstruction is not sufficiently high, the result shows that the proposed fitting algorithm is basically applicable to the reconstruction of the target with a finite size.

## 7. Comparison with the Conventional Aperture Synthesis

In this section, we compare the proposed algorithm based on the model fitting with the conventional aperture synthesis method in a quantitative manner.

Conventional aperture synthesis reconstructs the image at a position $\boldsymbol{x}$ with the following equation[9].

$$b(\boldsymbol{x}) = \int w(\boldsymbol{x}_r, 2|\boldsymbol{x}-\boldsymbol{x}_r|/c_u)\frac{y^3}{|\boldsymbol{x}-\boldsymbol{x}_r|^3}\,dx_r \qquad (10)$$

where $\boldsymbol{x}_r$ is the position of the antenna and $w(\boldsymbol{x}_r, t)$ is an output of the pulse compression filter. Since no clutter or noise is added in the simulation in this

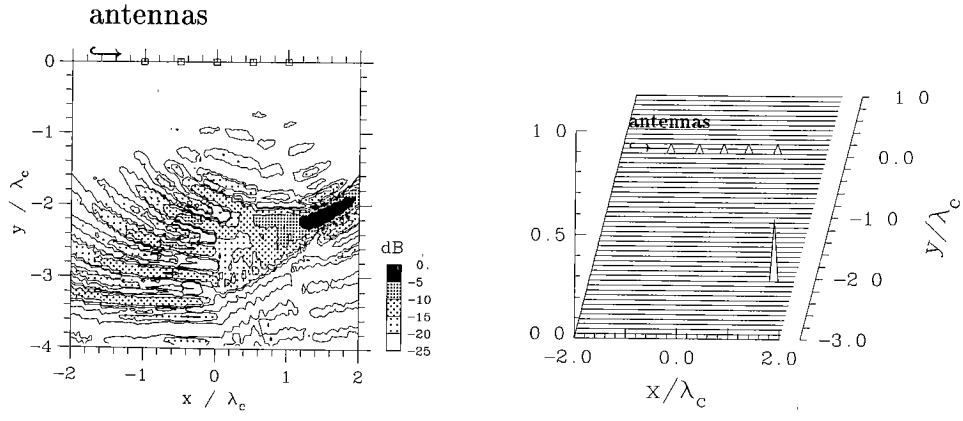


(a) (b)

**Fig. 12** Comparison with the conventional method.
(a) reconstructed image by the conventional aperture synthesis.
(b) reconstructed image by the fitting method.
The target model includes one point target.

section, the inverse filter is adopted as the pulse compression filter. We compare the reconstructed image by the fitting algorithm with the image calculated with Eq. (10).

Figure 12 shows an example of the reconstruction of one point target where SIR is 40 dB. The reconstructed image by the conventional method deteriorates seriously, and the image of the point target disperses with many spurious responses emerging at $x/\lambda_c = -1$-0. This deterioration is due to the restriction of the aperture size. On the other hand, the proposed fitting method focuses a sharp image under the same condition as shown in Fig. 12(b).

In order to compare these two methods quantitatively, we define the image width $W$ as the second moment of the reconstructed image around the estimated point.

$$W = \sum_{|r_0 - r_i| \leq \lambda_c} \{|r_0 - r_i|^2 |s_i|\} / \sum_{|r_0 - r_i| \leq \lambda_c} |s_i| \lambda_c^2 \qquad (11)$$

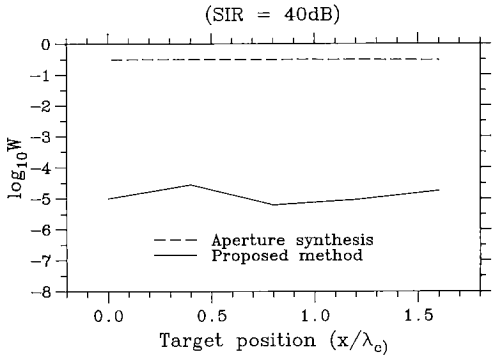


**Fig. 13** Comparison of the image widths calculated from the image of the fitting method and that of the conventional aperture synthesis. $y/\lambda_c = -2.0$.

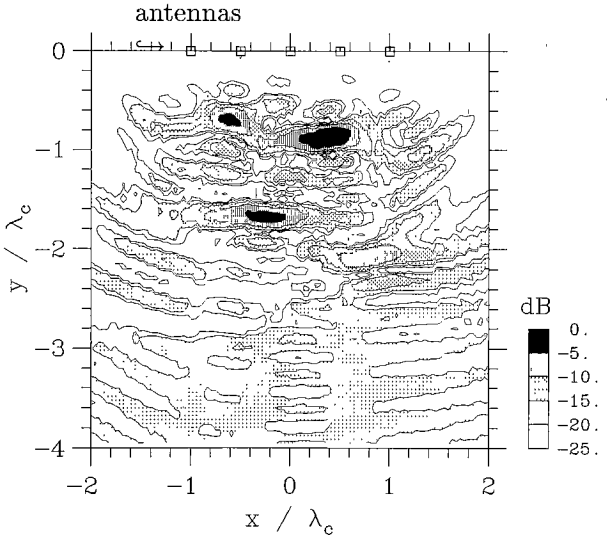


**Fig. 14** The reconstructed image by the conventional aperture synthesis. The model of the true image is the same as shown in Fig. 7(a).

where $r_0$ is the true position of the target and $s_i$ is the magnitude of the image at point $r_i$. Note that $W$ includes the error of estimated position of the target. The range of the summation in Eq. (11) is restricted by the threshold for the range between $r_0$ and $r_i$. This threshold excludes the images of clutter sources from $W$, and makes it possible to evaluate the image width properly. Figure 13 is the width of the reconstructed image versus the horizontal position of the target. The abscissa expresses the horizontal position of the target and the ordinate expresses the image width. The width of the reconstructed image by the fitting method is 40 dB smaller than that by the conventional method. This result shows that the fitting method focuses a much sharper image.

Figure 14 is the result of a case where 4 point targets exist. The image of the 4th target deteriorates seriously and can hardly be discriminated from spurious responses caused by other targets. Under the same condition, the proposed fitting algorithm clearly detects all 4 targets and no spurious response appears as shown in Fig. 7.

## 8. Conclusion

We proposed an algorithm of radar image reconstruction based on the model fitting, and showed its fundamental characteristics by a series of computer simulation. The model fitting is executed by nonlinear least-squares. The penalty function is added to the residual to make the algorithm stable under the existence of clutters around targets.

The comparison with the conventional aperture synthesis showed an improvement of about 40 dB in the width of the reconstructed images. In the fitting algorithm, restriction of the number of point targets, which is especially efficient when the size of the antenna array is limited, reduces the spurious response and sharpens the target image.

Though the proposed algorithm assumes that the medium is homogeneous, the medium is generally inhomogeneous in an actual situation. The performance of the algorithm will deteriorate when it is applied to the actual radar observation. The relation between the degree of inhomogeneity and deterioration of the performance of the proposed method must be examined, and the measures against the inhomogeneity should be taken in the future studies. Since our algorithm is to solve the inverse problem by iterating the forward problem, it is, in principle, possible to take the inhomogeneity directly into account. We intend to extend the proposed algorithm to cases where medium has simple inhomogeneity, such as multiple layers, by including the medium parameters into the unknowns.

## References

[1] Wernecke, S. J. and D'Addario, L. R., "Maximum Entropy Image Reconstruction," *IEEE Trans. Comput*, vol. C-26, no. 4, 1977.
[2] Furusawa, A., Wakayama, T., Sato, T. and Kimura, I., "Two-dimensional Interpolation in the Wavenumber Domain for Radar Image Reconstruction," *Trans. IEICE*, vol. J76-B II, no. 4, 1993.
[3] Chiu, S., Kanasewich, E. and Phadke, S., "Three-dimensional determination of structure and velocity by seismic tomography," *Geophisics*, vol. 51, no. 8, pp. 1559–1571, 1986.
[4] Mostafavi, M. and Mittra, R., "Remote probing of inhomogeneous media using parameter optimization techniques," *Radio Science*, vol. 7, no. 12, pp. 1105–1111, 1972.
[5] Lesselier, D., "Optimization techniques and inverse problems: reconstruction of conductivity profiles in the time domain", *IEEE Trans. Antennas & Propag.*, vol. AP-30, no. 1, pp. 59–65, 1982.
[6] Uno, T. and Adachi, S., "Inverse Scattering Method for One-Dimensional Inhomogeneous Layered Media," *IEEE Trans. Antennas & Propag.*, vol. AP-35, no. 12, pp. 1456–1466, 1987.
[7] Wolf, E., "Three-dimensional Structure Determination of Semi-transparent Object From Holographic Data," *Optics Communications*, vol. 1, no. 4, 1966.
[8] Vanmarke, E., *Random Fields: Analysis and Synthesis*," MIT Press, 1983.
[9] Osumi, N. and Ueno, K., "Microwave Holographic Imaging Method with Improved Resolution," *IEEE Trans. Antennas & Propag.*, vol. AP-32, no. 10, pp. 1018–1026, 1984.
[10] Marquardt, D. W., "An Algorithm for Least Squares Estimation of Nonlinear Parameters," *J. Soc. Indust. Appl. Math.*, vol. 11, pp. 431–441, 1963.
[11] Shigesawa, H., "Equivalent Source Method," in *Analysis Method for Electromagnetic Wave Problems*, ed. Yamashita E., Ch. 6, Artech House, 1990.

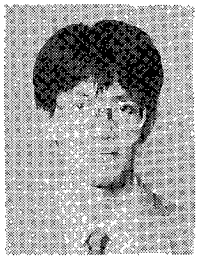

**Toshio Wakayama** received the B.E. and M.E. degrees from Kyoto University, Japan in 1990 and 1992, respectively. He is currently working toward Dr.E degree at Department of Electrical Engineering II, Kyoto University. His research interest is radar image reconstruction.

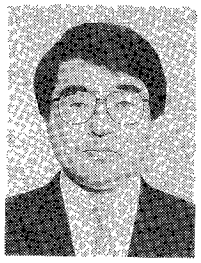

**Toru Sato** received the B.E., M.E., and Ph.D. degrees in electrical engineering from Kyoto University, Kyoto, Japan in 1976, 1978, and 1982, respectively. He was a graduate student research associate of Arecibo Observatory, National Astronomy and Ionosphere Center from 1979 to 1980. He joined Radio Atmospheric Science Center of Kyoto University in 1983 as a research associate. He has been a lecturer at Department of Electrical Engineering II, Kyoto University since 1988. His major research interests have been system design and signal processing for atmospheric radars, radar remote sensing of the atmosphere, observations of precipitation using radar and satellite signals, radar observation of space debris, signal processing for subsurface radars, and digital satellite communication. He was awarded Tanakadate Prize in 1986. He is a member of the Society of Geomagnetism and Earth, Planetary and Space Sciences, the Japan Society for Aeronautical and Space Sciences, the Institute of Electrical and Electronics Engineers, and American Meteorological Society.

**Iwane Kimura** received the B.E., M.E., and Ph.D. degrees in electrical engineering from Kyoto University, Kyoto, Japan in 1955, 1957, and 1961 respectively. Since 1960, he has been a staff of Kyoto University; Department of Electronics and Department of Electrical Engineering II where he is now a Professor radio engineering since 1971. He has also been a visiting Professor of Institute of Space and Astronautical Science from 1981 to 1991. From 1964 to 1965, he was a research associate at Radioscience Laboratory, Stanford University on leave from Kyoto University. His research interests have been in radio science; particularly remote-sensing of upper atmospheres by radar techniques, and space plasma physics, such as theoretical study on propagation and generation of radio waves in magnetospheric and ionospheric plasmas, plasma measurements by rocket-Doppler technique, and active wave experiments in space plasmas using scientific statellites. He was awarded Inada Memorial Prize in 1958, and Tanakadate Prize in 1961. He is a member of the Institute of Electrical Engineers of Japan, the Society of Geomagnetism and Earth, Planetary and Space Sciences, and the American Geophysical Union.